 CMES, vol.119, no.1, pp.125-143, 2019

An IB Method for Non-Newtonian-Fluid Flexible-Structure Interactions in Three-Dimensions

Luoding Zhu[1,*]

Abstract: Problems involving fluid flexible-structure interactions (FFSI) are ubiquitous in engineering and sciences. Peskin's immersed boundary (IB) method is the first framework for modeling and simulation of such problems. This paper addresses a three-dimensional extension of the IB framework for non-Newtonian fluids which include power-law fluid, Oldroyd-B fluid, and FENE-P fluid. The motion of the non-Newtonian fluids are modelled by the lattice Boltzmann equations (D3Q19 model). The differential constitutive equations of Oldroyd-B and FENE-P fluids are solved by the D3Q7 model. Numerical results indicate that the new method is first-order accurate and conditionally stable. To show the capability of the new method, it is tested on three FFSI toy problems: a power-law fluid past a flexible sheet fixed at its midline, a flexible sheet being flapped periodically at its midline in an Oldroyd-B fluid, and a flexible sheet being rotated at one edge in a FENE-P fluid.

Keywords: Fluid flexible-structure interaction, immersed boundary method, lattice Boltzmann, power-law, Oldroyd-B, FENE-P.

1 Introduction

Phenomena of fluid flexible-structure interactions (FFSI) are ubiquitous in various fields of engineering and sciences. For instances, clothes moving in a washing machine, booms floating in ocean preventing oil pollution, blood flowing in deformable blood vessels, to name just a few. Due to complexity of such problems, mathematical modeling and computer simulation of FFSI problems are challenging. The first methodology for modeling and simulation of FFSI problems is probably the immersed boundary (IB) method introduced by Peskin [Peskin (1972, 1973)]. Since the birth of the IB method, numerous methods for FFSI problems are developped. These include immersed boundary method [Iaccarino and Verzicco (2003); Mittal and Iaccarino (2005)], Arbitrary Lagrangian Eulerian (ALE) [Hughes, Liu and Zimmermann (1981); Donea, Giuliani and Halleux (1982); Yang, Sun, Wang et al. (2016)], the lattice Boltzmann [Lallemand and Luo (2003)], fictitious domain [Glowinski, Pan and Periaux (1994a,b)], front tracking [Glimm, Grove, Li et al. (1998)], immersed interface [Leveque and Li (1994); LeVeque and Li (1997); Li and Lai (2001)], blob-projection [Cortez (2000)], phase field [Sun, Xu and Zhang (2014); Wick (2016); Zheng and Karniadakis (2016); Mokbel, Abels and Aland (2018)], immersed

[1]Indiana University-Purdue University Indianapolis, USA.
[*]Corresponding Author: Luoding Zhu. Email: luozhu@iupui.edu.

finite element [Zhang, Gerstenberger, Wang et al. (2004); Liu, Tang et al. (2007)], material points [Sulsky, Chen and Schreyer (1994); Sulsky, Zhou and Schreyer (1995)], immersed continuum [Wang and Liu (2004); Wang (2006)], the level set [Hou, Li, Osher et al. (1997); Xu, Li, Lowengrub et al. (2006); Cottet and Maitre (2006)], the gas-kinetic [Jin and Xu (2008)], and monolithic approach [Hübner, Walhorn and Dinkler (2004); Hron and Turek (2006); Barker and Cai (2010)].

Because of complexity and diversity of FFSI problems and limitations of mathematics and computer technology, the immersed boundary method has had many different variants designed specifically for FFSI problems with various peculiar features. Examples include the original versions [Peskin (1972, 1977); Peskin and McQueen (1996)], the compressible fluid version [Wang, Currao, Han et al. (2017)], the fluid-solute version [Lee, Griffith and Peskin (2010)], the rigid body version [Kim and Peskin (2016)], the thick rod version [Lim, Ferent, Wang et al. (2008)], the volume-conservation version [Peskin and Printz (1993); Rosar and Peskin (2001)], the poroelastic version [Strychalski, Copos, Lewis et al. (2015)], the adaptive mesh-refinement [Roma, Peskin and Berger (1999); Griffith, Hornung, McQueen et al. (2007)], the porous media [Stockie (2009)], the formally 2^{nd}-order [Lai and Peskin (2000); Griffith and Peskin (2005)], the multigrid [Zhu and Peskin (2002); Zhu and Chin (2008)], the penalty [Kim and Peskin (2007)], the finite element [Boffi and Gastaldi (2003); Boffi, Gastaldi, Heltai et al. (2008); Griffith and Luo (2012); Hua, Zhu and Lu (2014)], the stochastic [Atzberger, Kramer and Peskin (2007); Atzberger and Kramer (2008)], the lattice-Boltzmann [Feng and Michaelides (2004, 2005); Zhu, He, Wang et al. (2011a); Tian, Luo, Zhu et al. (2011); Cheng and Zhang (2010); Wu and Shu (2009); Shu, Liu and Chew (2007); Niu, Shu, Chew et al. (2006); Wu, Shu and Zhang (2010); Cheng, Zhu and Zhang (2014); Liu, Peng, Liang et al. (2012); Zhang, Cheng, Zhu et al. (2016)], the variable viscosity version [Fai, Griffith, Mori et al. (2013, 2014)], the vortex-method version [McCracken and Peskin (1980)], the implicit versions [Fauci and Fogelson (1993); Taira and Colonius (2007); Mori and Peskin (2008); Hou and Shi (2008); Newren, Fogelson, Guy et al. (2008); Hao and Zhu (2010, 2011)],

Newtonian fluids are assumed for most of the existing versions of the IB method. However, FFSI problems may involve non-Newtonian fluids. For instance, cytoplasm interacting with cytoskeleton in a living cell; blood interacting with red/white cells in a blood vessel; and poroelastic tissue interacting with a cancer cell during metastasis. Many special properties are displayed by non-Newtonian fluids including normal stress differences and shear thinning/thickening. In contrast to Newtonian fluids which may be described by a universal strain-stress equation; there exists no universal constitutive equation for all non-Newtonian fluids. Different non-Newtonian fluids have to be described by different constitutive equations (algebraic or differential) characterizing history effects and strain-stress relationships.

Note that the existing non-Newtonian immersed boundary methods [Chrispell, Cortez, Khismatullin et al. (2011); Chrispell, Fauci and Shelley (2013); Tian (2016); Zhu, Yu, Liu et al. (2017)] are for power-law or Oldroyd-B fluids in two-dimensions except [Zhu, Yu, Liu et al. (2017)] which is three-dimensional for power-law fluids. Tian et al. [Ma, Wang,

John et al. (2018)] are developping an immersed-boundary lattice-Boltzmann method for viscoelastic fluids including Oldroyd-B and FENE-CR fluids. In their work the motion equations of the solid are solved for by finite difference or finite element methods. In this paper we discuss our recent development of a 3D IB methods for three non-Newtonian fluids: power-law, Oldrod-B [Oldroyd (1950)], and FENE [Peterlin (1961)]. These models can describe many non-Newtonian fluids encountered in real-world problems including blood and polymeric fluids. Some preliminary results was reported in a short letter [Zhu (2018)]. Details and more tests of the new method, including the integration of the three non-Newtonian models are presented in the current paper.

In our new method, the lattice Boltzmann equations, the D3Q19 model [Qian (1990); SY and GD (1998)], are used to model the fluid flow. The power-law, the Oldroyd-B model, and the FENE-P model are used to model constitutive equations for various non-Newtonian fluids. The formal one (power-law) is incorporated into the lattice Boltzmann D3Q19 model by an algebraic approach; the latter two are numerically solved by the lattice Boltzmann D3Q7 model [Malaspinas, Fiétier and Deville (2010)]. The deformable structure is modelled by elastic fibers which can be stretched, compressed, and bent. The fluid-structure-interaction is modelled by the Dirac delta function, as in Peskin's original immersed boundary method. Note that in our method, the three non-Newtonian models are integrated seamlessly via a model parameter. Selection of a specific model is done by setting a specific numerical value to the parameter. This is a unique feature of our hybrid method thanks to the advantages of using lattice Boltzmann approach for modeling both fluid motions and the corresponding constitutive equations.

To examine the new method and demonstrate its capability, we consider three FFSI toy problems- a power-law fluid flow passes a deformable sheet tethered at the middleline, a flexible rectangular sheet is flapped sinusoidally at its midline in a stationary Oldroyd-B fluid, and a flexible rectangular sheet is rotated at one edge in a stationary FENE-P fluid.

The remaining article is as follows. Section 2 gives the complete mathematical formulation of the IB method for non-Newtonian fluids. Section 3 discusses details of the numerical methods for the mathematical formulation. Section 4 addresses the verification and validation of the new method and its implementation. Section 5 reports some main simulation results for each of the three test problems. Section 6 concludes the paper with a summary.

2 Mathematical formulation

The immersed boundary formulation, a nonlinear system of differential-integral equations, describing the motion of a generic flexible structure in a non-Newtonian fluid (power-law, Oldroyd-B or FENE-P) may be written as follows. The equations are listed first and then followed by explanation.

$$\rho\left(\frac{\partial \mathbf{u}}{\partial t}+\mathbf{u}\cdot\nabla\mathbf{u}\right)=-\nabla p+\nabla\cdot(2\eta\mathbf{D})+\nabla\cdot\mathbf{\Pi}+\boldsymbol{f}_{ib}(\boldsymbol{x},t)+\boldsymbol{b}_f(\boldsymbol{x},t), \tag{1}$$

$$\nabla \cdot \mathbf{u} = 0, \tag{2}$$

$$\eta(\dot{\gamma}) = \eta_0(\dot{\gamma})^{n-1}, \quad \dot{\gamma} = \sqrt{2D_{ij}D_{ij}}, \quad D_{ij} = \frac{1}{2}(u_{ij} + u_{ji}), \tag{3}$$

$$\mathbf{\Pi} = \frac{\mu_p}{\kappa_p}(a\mathcal{C} - b\mathbf{I}), \quad \frac{\partial \mathcal{C}}{\partial t} + \mathbf{u} \cdot \nabla \mathcal{C} = -\frac{1}{\kappa}(a\mathcal{C} - b\mathbf{I}) + \mathcal{C} \cdot \nabla \mathbf{u} + (\nabla \mathbf{u})^T \cdot \mathcal{C} \tag{4}$$

$$a = \frac{1}{1 - tr(\mathcal{C})/r_p^2}, \quad b = \frac{1}{1 - 3/r_p^2} \tag{5}$$

$$\boldsymbol{f}_{ib}(\boldsymbol{x}, t) = \int_\Gamma \boldsymbol{F}(\boldsymbol{\alpha}, t)\delta(\boldsymbol{x} - \boldsymbol{X}(\boldsymbol{\alpha}, t))d\boldsymbol{\alpha} \tag{6}$$

$$\mathbf{F}(\boldsymbol{\alpha}, t) = -\frac{\partial \mathcal{E}}{\partial \mathbf{X}} = -\frac{\partial(\mathcal{E}_s + \mathcal{E}_b)}{\partial \mathbf{X}} \tag{7}$$

$$\mathcal{E}_s = \frac{1}{2}K_s \int \left(\left| \frac{\partial \mathbf{X}(\boldsymbol{\alpha}, \mathbf{t})}{\partial \boldsymbol{\alpha}} \right| - 1 \right)^2 d\boldsymbol{\alpha}, \quad \mathcal{E}_b = \frac{1}{2}K_b \int \left| \frac{\partial^2 \mathbf{X}(\boldsymbol{\alpha}, t)}{\partial \boldsymbol{\alpha}^2} \right|^2 d\boldsymbol{\alpha} \tag{8}$$

$$\frac{\partial \mathbf{X}}{\partial t}(\boldsymbol{\alpha}, t) = \mathbf{U}(\boldsymbol{\alpha}, t) \tag{9}$$

$$\boldsymbol{U}(\boldsymbol{\alpha}, t) = \int_\Gamma \boldsymbol{u}(\boldsymbol{x}, t)\delta(\boldsymbol{x} - \boldsymbol{X}(\boldsymbol{\alpha}, t))\mathrm{d}\boldsymbol{x}. \tag{10}$$

Eqs. (1) and (2) are the classic Navier-Stokes equations for a viscous incompressible fluid where $\mathbf{u}$ denotes the fluid velocity, ρ denotes the density, p the pressure. The symbol $\boldsymbol{f}_{ib}$ denotes the Eulerian force applied by the immersed structure to the fluid, $\boldsymbol{b}_f$ denotes other external forces exerted on the fluid, for example, the gravity. The letter $\mathbf{D} = (\nabla \mathbf{u} + \nabla \mathbf{u}^T)/2$ denotes the strain rate tensor, η the fluid dynamic viscosity, and $\mathbf{\Pi}$ the viscoelastic stress tensor. Note that the two equations are valid for both Newtonian and non-Newtonian fluids. For Newtonian fluids, η is constant and $\mathbf{\Pi}$ is zero. For non-Newtonian fluids obeying power-law, η is given by Eq. (3) where $\dot{\gamma}$ is the shear rate, D_{ij} is the ij^{th} component of strain rate tensor, constants η_0 and n are model parameters describing the properties of the non-Newtonian fluid. Note that when $n = 1$ the fluid becomes Newtonian. For non-Newtonian fluids such as polymeric fluids, the viscoelastic stress $\mathbf{\Pi}$ may be computed from the conformation tensor $\mathcal{C}$ (Eq. (4)), where κ_p and μ_p are the relaxation time and dynamical viscosity of the polymer, respectively. The polymer conformation tensor $\mathcal{C}$ is governed by

Eq. (4) , i.e., the FENE-P model [Peterlin (1961)]. The variables a and b are given by Eq. (5) where r_p is a model parameter related to the maximum length of polymer molecules which is permitted and $tr(\mathcal{C})$ is the trace of the conformation tensor $\mathcal{C}$. Note that variable a is a nonlinear function of the conformation tensor $\mathcal{C}$ and the FENE-P model is a nonlinear system of hyperbolic partial differential equations. When $a = b = 1$, FENE-P model reduces to the popular linear Oldroyd-B model [Oldroyd (1950)]. Note that the Navier-Stokes equations are parabolic and elliptic in nature, but the FENE-P model (Eq. (4)) is hyperbolic. They are coupled through fluid velocity $\mathbf{u}$ and viscoelastic force $\mathbf{\Pi}$.

The immersed boundary Eulerian force density $\boldsymbol{f}_{ib}$ in Eqs. (1) and (2) can be computed via Eq. (6), where $\boldsymbol{\alpha}$ is the Lagrangian coordinate of the immersed structure. The function δ is the classic Dirac delta function. The symbol $\boldsymbol{X}$ is Lagrangian position of the structure. The function $\mathbf{F}$ is the corresponding Lagrangian force density, which is computed from the elastic potential energies (Eq. (8)) of the structure. In Eq. (8), the first integral represents the contribution from stretching/compression ($\mathcal{E}_s$) and the second one represents the contribution from bending ($\mathcal{E}_b$). The quantities K_b and K_s are bending and stretching coefficients of the elastic constitutive fibers of the deformable structure. Their numerical values are related to the Youngs' modulus and Poisson ratio of the structure [Strychalski, Copos, Lewis et al. (2015)]. The velocity of the immersed structure $\boldsymbol{U}(\boldsymbol{\alpha}, t)$ is interpolated from the velocity of surrounding fluid by Eq. (10). Note that this equation by definition dictates that the immersed structure must follow the motion of fluid because of fluid viscosity. That is, the no-slip boundary condition is enforced on the fluid-solid interface.

There are three major dimensionless ratios in the FFSI problems involving non-Newtonian fluids: Reynolds number $Re = \frac{U_c L_c}{\nu_p + \nu_f}$, structure flexure modulus $\hat{K_b} = \frac{K_b}{\rho_c U_c^2 L_c^4}$, and Weissenberg number for polymeric fluid $Wi = \kappa_p \dot{\gamma}$ (or exponent n for power-law fluid). In above definition, ρ_c is the characteristic fluid mass density, U_c is the characteristic flow speed, L_c is the characteristic length of the immersed structure, κ_p is the relaxation time of polymer, $\dot{\gamma}$ is the characteristic flow shear rate, ν_p is the polymer kinematic viscosity, and ν_f is the fluid kinematic viscosity. Note that Re measures the ratio of inertial force and viscous force, $\hat{K_b}$ measures the ratio of the elastic force and inertial force, Wi measures the ratio of viscoelastic force and viscous force. The index of power-law $n < 1$ corresponds to shear-thinning fluid, $n > 1$ corresponds to shear-thickening fluid, and $n = 1$ corresponds to Newtonian fluid.

3 Numerical methods

As we can see, the immersed boundary formulation for the FFSI problems of non-Newtonian fluids is a nonlinear system of integral and partial differential equations (PDE). The PDEs are of mixed type (hyperbolic, parabolic, and elliptic). Numerical solution of this kind of hybrid system is challenging. Here we choose to use the lattice Boltzmann approach [Wolf-Gladrow (2000); Guo and Shu (2013); Huang, Sukop and Lu (2015); Succi (2018)] for this system. The lattice Boltzmann approach treats the incompressible flows as slightly compressible flows (which are governed by hyperbolic PDEs). This

kind of artificial compressibility approach for the flow equations is consistent with the hyperbolic nature of the constitutive equations of the non-Newtonian fluids such as FENE-P fluids. The details of the discretizations for the flow equations, constitutive equations, and immersed boundary equations are given as below.

The lattice Boltzmann equations, the D3Q19 model [Qian (1990); SY and GD (1998)], are used to solve numerically the viscous incompressible flow equations (Eqs. (1) and (2)) for non-Newtonian fluids. Carefully chosen 19 velocities (with three speeds) are used to discretize the particle velocity space $\boldsymbol{\xi}$, $\boldsymbol{\xi}_i$ $(i = 0, 1, ..., 18)$:

$$\boldsymbol{\xi}_i = \begin{cases} (0,0,0), & i = 0 \\ (\pm 1,0,0),(0,\pm 1,0),(0,0,\pm 1), & i = 1,2,...,6 \\ (\pm 1,\pm 1,0),(\pm 1,0,\pm 1),(0,\pm 1,\pm 1), & i = 7,8,...,18. \end{cases}$$

Use $g_i(\mathbf{x}, t)$ to denote the single-particle velocity distribution function along the direction of $\boldsymbol{\xi}_i$ $(i = 0, 1, ..., 18)$. The lattice Boltzmann equation (LBE) advancing $g_i(\mathbf{x}, t)$ one-time-step forward along the direction $\boldsymbol{\xi}_i$ can be written as

$$g_i(\mathbf{x}+\boldsymbol{\xi}_i, t+1) = g_i(\mathbf{x}, t) - \frac{1}{\tau}(g_i(\mathbf{x}, t) - g_i^{(eq)}(\mathbf{x}, t)) + (1 - \frac{1}{2\tau})w_i(\frac{\boldsymbol{\xi}_i - \mathbf{u}}{{c_s}^2} + \frac{\boldsymbol{\xi}_j \cdot \mathbf{u}}{{c_s}^4}\boldsymbol{\xi}_i) \cdot \mathbf{f}_t \tag{11}$$

Here $\mathbf{f}_t = \mathbf{f}_{ib} + \nabla \cdot \mathbf{\Pi} + \mathbf{f}_\mathbf{b}$. The relaxation time τ is related to the fluid kinematic viscosity ν_f by $\tau = \frac{6\nu_f + 1}{2}$ (note $\nu_f = \eta/\rho$). The weight w_i is given as follows:

$$w_i = \begin{cases} 1/3, & i = 0 \\ 1/18, & i = 1,2,...,6 \\ 1/36, & i = 7,8,...,18. \end{cases}$$

Here $c_s = c/\sqrt{3}$ is the model sound-speed and c is the model lattice-speed:

$$c = \begin{cases} 0, & i = 0 \\ 1, & i = 1,2,...,6 \\ \sqrt{2}, & i = 7,8,...,18. \end{cases}$$

The function $g_i^{(eq)}$ is the discretization of the equilibrium distribution function:

$$g_i^{(eq)}(\mathbf{x}, t) = \rho(\mathbf{x}, t)w_i(1 + 3\boldsymbol{\xi}_i \cdot \mathbf{u}(\mathbf{x}, t) + \frac{9}{2}(\boldsymbol{\xi}_i \cdot \mathbf{u}(\mathbf{x}, t))^2 - \frac{3}{2}\mathbf{u}(\mathbf{x}, t) \cdot \mathbf{u}(\mathbf{x}, t)) \tag{12}$$

The method introduced in Guo et al. [Guo, Zheng and Shi (2002)] is applied to treat the external force term. Note that the lattice Boltzmann equation (Eq. (11)) can be regarded as an explicit second-order accurate discretization in space and time of the flow equations for viscous non-Newtonian fluids by a Lagrangian approach [Wolf-Gladrow (2000)]. It is equivalent to a second-order finite difference scheme for the viscous incompressible Navier-Stokes equations [Junk (2001)].

For non-Newtonian fluids modelled by power law, the constitutive equation is incorporated into the lattice Boltzmann flow model (the D3Q19) algebraically by Eq. (3). The shear rate may be calculated as follows: $\dot{\gamma} = \sqrt{2D_{ij}D_{ij}}$, D_{ij} $(i = 1, 2, 3; j = 1, 2, 3)$ is computed by $D_{ij} = -\frac{3}{2\tau}\sum_{k=0}^{k=18}\xi_{ki}\xi_{kj}g_k^{(1)}$, where $g_k^{(1)} = g_k - g_k^{(eq)}$. Here g_k is the velocity distribution function along k^{th} direction, $g_k^{(eq)}$ is the equilibrium distribution function, and ξ_{ki} $(k = 0, 1, ..., 18; i = 1, 2, 3)$ is the i^{th} component of the k^{th} discrete direction. See [Zhu, Yu, Liu et al. (2017)] for details.

For non-Newtonian fluids whose constitutive laws obeying the FENE-P model (including the Oldroyd-B model), the lattice Boltzmann D3Q7 model for advection-diffusion equations [Malaspinas, Fiétier and Deville (2010)] is applied for numerical solutions of their constitutive equations. It is coupled with the lattice Boltzmann model for flow equations through the flow velocity $\mathbf{u}$ and viscoelastic force $\mathbf{\Pi}$. Lattice Boltzmann particles in the D3Q7 model are allowed to move along six discrete directions $\boldsymbol{\zeta}_i, i = 1, 2, ..., 6$ at a node, where

$$\boldsymbol{\zeta}_i = \begin{cases} (\pm 1, 0, 0) & i = 1, 2 \\ (0, \pm 1, 0) & i = 3, 4 \\ (0, 0, \pm 1) & i = 5, 6. \end{cases}$$

Particles can also stay at the node $\boldsymbol{\zeta}_0 = (0, 0, 0)$. For a given component of the configuration tensor $\mathcal{C}_{\alpha\beta}$, at a given node $\mathbf{x}$, along a given direction $\boldsymbol{\zeta}_i, i = 0, 1, 2, ..., 6$, the single-particle velocity distribution function $q_{\alpha\beta i}$ is evolved according to

$$q_{\alpha\beta i}(\mathbf{x}+\boldsymbol{\zeta}_i, t+1) - q_{\alpha\beta i}(\mathbf{x}, t) = -\frac{1}{\chi}(q_{\alpha\beta i}(\mathbf{x}, t) - q_{\alpha\beta i}^{(eq)}(\mathcal{C}_{\alpha\beta}, \mathbf{u})) + (1 - \frac{1}{2\chi})\frac{\psi_{\alpha\beta}}{\mathcal{C}_{\alpha\beta}}q_{\alpha\beta i}^{(eq)}(\mathcal{C}_{\alpha\beta}, \mathbf{u}). \tag{13}$$

Where the relaxation time χ is related to the diffusivity constant κ_p by $\chi = \frac{8\kappa_p+1}{2}$. The ratio κ_p/μ_p is set to be a very small number e.g. 10^{-6}, here μ_p is polymer dynamical viscosity. The equilibrium distribution $q_{\alpha\beta i}^{(eq)} = w_i\mathcal{C}_{\alpha\beta}(1 + \frac{\zeta_{ik}u_k}{c_i^2})$, where ζ_{ik} is the k^{th} $(k = 1, 2, 3)$ component of velocity $\boldsymbol{\zeta}_i$ $(i = 0, 1, 2, ..., 6)$. Function $\psi_{\alpha\beta} = -\frac{1}{\kappa_p}(a\mathcal{C}_{\alpha\beta} - b\delta_{\alpha\beta}) + \mathcal{C}_{\alpha i}\frac{\partial u_\beta}{\partial x_i} + \mathcal{C}_{i\beta}\frac{\partial u_\alpha}{\partial x_i}$. The $\alpha\beta^{th}$ component of the conformation tensor is computed by $\mathcal{C}_{\alpha\beta} = \sum_{i=0}^{i=6} q_{\alpha\beta i} + \frac{1}{2}\psi_{\alpha\beta}$. The viscoelastic force in Eq. (1) is computed by $\nabla \cdot \mathbf{\Pi} = \nabla \cdot (\frac{\mu_p}{\kappa_p}(a\mathcal{C} - b\mathbf{I}))$ and the spatial derivative $\partial_{x_i}, i = 1, 2, 3$ is discretized by the central difference scheme.

The macroscopic fluid mass density $\rho(\mathbf{x}, t)$ and momentum (hence velocity) $\rho\mathbf{u}(\mathbf{x}, t)$ can be computed from $g_i(\mathbf{x}, t)$ at each node by

$$\rho(\mathbf{x}, t) = \sum_i g_i(\mathbf{x}, t), \tag{14}$$

$$(\rho\mathbf{u})(\mathbf{x},t)=\sum_i \boldsymbol{\xi}_i g_i(\mathbf{x},t)+\frac{\mathbf{f}_t(\mathbf{x},t)}{2}. \tag{15}$$

Let integer m denote time step: $g^m = g(\mathbf{x},\boldsymbol{\xi},m)$, $\mathbf{X}^m(\boldsymbol{\alpha}) = \mathbf{X}(\boldsymbol{\alpha},m)$, $\mathbf{u}^m = \mathbf{u}(\mathbf{x},m)$, $p^m = p(\mathbf{x},m)$, $\rho^m = \rho(\mathbf{x},m)$. Let the flexible structure be discretized by a set of elastic fibers with Lagrangian coordinate α_2. Let $\alpha_2 = k_2\Delta\alpha_2$, where k_2 is an integer. Let a fiber be discretized by a set of points with Lagrangian coordinate α_1. Let $\alpha_1 = k_1\Delta\alpha_1$, where k_1 is an integer.

Then the elastic potential energy is discretized by:

$$\mathcal{E}=\frac{1}{2}K_s\sum_{k=1}^{N_f-1}(\frac{|\mathbf{X}_{k+1}-\mathbf{X}_k|}{\Delta\alpha_1}-1)^2\Delta\alpha_1+\frac{1}{2}K_b\sum_{k=2}^{N_f-1}\frac{|\mathbf{X}_{k+1}+\mathbf{X}_{k-1}-2\mathbf{X}_k|^2}{(\Delta\alpha_1)^4}\Delta\alpha_1. \tag{16}$$

where the first term corresponds to the stretching/compression energy and the second term corresponds to the bending energy. The Lagrangian force density at node with index l, $(\mathbf{F})_l$, $l = 1, 2, ..., N_f$, is given by

$$\begin{aligned}(\mathbf{F})_l=&\frac{K_s}{{\Delta\alpha_1}^2}\sum_{k=1}^{N_f-1}(|\mathbf{X}_{k+1}-\mathbf{X}_k|-\Delta\alpha_1)\frac{\mathbf{X}_{k+1}-\mathbf{X}_k}{|\mathbf{X}_{k+1}-\mathbf{X}_k|}(\delta_{kl}-\delta_{k+1,l})\\&+\frac{K_b}{(\Delta\alpha_1)^4}\sum_{k=2}^{N_f-1}(\mathbf{X}_{k+1}+\mathbf{X}_{k-1}-2\mathbf{X}_k)(2\delta_{kl}-\delta_{k+1,l}-\delta_{k-1,l}).\end{aligned} \tag{17}$$

Here δ_{kl} is the Kronecker δ: $\delta_{kl} = 1$ if $k = l$ and $\delta_{kl} = 0$ if $k \neq l$. The integral equations in the immersed boundary formulation are computed by the trapezoidal rule:

$$\mathbf{f}_{ib}^{m+1}(\mathbf{x})=\sum_{\Gamma}\mathbf{F}^{m+1}(\boldsymbol{\alpha})\delta_d(\mathbf{x}-\mathbf{X}^m(\boldsymbol{\alpha}))\Delta\boldsymbol{\alpha} \tag{18}$$

$$\mathbf{U}^{m+1}(\boldsymbol{\alpha})=\sum_{\Omega}\mathbf{u}^{m+1}(\mathbf{x})\delta_d(\mathbf{x}-\mathbf{X}^m(\boldsymbol{\alpha}))\Delta x\Delta y\Delta z \tag{19}$$

Here Γ denotes the immersed structure, Ω denotes the fluid domain. And $\Delta x, \Delta y$, and Δz denote the meshwidth in x, y, and z directions. The Dirac δ function is discretized by δ_d:

$$\delta_d(\mathbf{x})=\frac{1}{\Delta x\Delta y\Delta z}\phi(\frac{x}{\Delta x})\phi(\frac{y}{\Delta y})\phi(\frac{z}{\Delta z}) \tag{20}$$

Here $\phi(r) = 0.25(1 + \cos(0.5\pi r))$ for $|r| \leq 2$ and is 0 otherwise. For other choices of $\phi(r)$ see Peskin et al. [Peskin and McQueen (1996)].

The motion equation of the structure is discretized by

$$\frac{\mathbf{X}^{m+1}(\boldsymbol{\alpha})-\mathbf{X}^m(\boldsymbol{\alpha})}{\Delta t}=\mathbf{U}^{m+1}(\boldsymbol{\alpha}) \tag{21}$$

For clarity the algorithm of the IB formulation for non-Newtonian fluids is summarized as follows. Suppose all variables are known at time step t (an integer), the procedure for updating all of the variables for next time step t+1 is as follows.

0) Initialization of all variables;

1) Advance the LBE (Eq. (11)) for flow (D3Q19 model) from t to t+1 using $\mathbf{f}_{ib}$ and $\mathbf{\Pi}$ from time step t; compute the new fluid velocity $\mathbf{u}$, velocity gradient $\nabla\mathbf{u}$, and mass density ρ;

2) Advance the LBE (Eq. (13)) for the constitutive equations (the D3Q7 model) from t to t+1 using $\mathbf{u}$ and $\mathcal{C}$ from time step t; compute the viscoelastic force $\nabla \cdot \mathbf{\Pi}$ from the newly updated conformation tensor $\mathcal{C}$,

3) Compute the structure velocity $\mathbf{U}$ from the fluid velocity $\mathbf{u}$ by Eq. (19);

4) Update the structure position by its velocity via Eq. (21);

5) Compute the immersed boundary force exerted by the structure to the fluid using its new configuration via Eq. (17);

6) Convert the Lagrangian force to Eulerian force by Eq. (18);

7) Compute the new equilibrium distribution functions of the $q_{\alpha\beta}^{(eq)}$ and $g^{(eq)}$ using the newly obtained fluid velocity $\mathbf{u}$, conformation tensor $\mathcal{C}$, and mass density ρ;

8) Go to 1).

Note that the algorithm for non-Newtonian fluids can be easily combined with algorithm for Newtonian fluids using the D3Q19 model. Therefore, the new method may be implemented in one computer program with a single model parameter m_p (an integer) to switch between Newtonian and non-Newtonian fluids. The option $m_p = 0$ selects Newtonian fluid. The code will bypass the D3Q7 model and set $\mathbf{\Pi} = 0$, $n = 1$. The option $m_p = 1$ selects the power-law fluid. The code will bypass the D3Q7 model and set $\mathbf{\Pi} = 0$. The option $m_p = 2$ selects the Oldroyd-B fluid. The code will execute the D3Q7 model with $a = b = 1$ and set $n = 1$. The option $m_p = 3$ selects the FENE-P fluid. The code will execute the D3Q7 model and set $n = 1$. Thus the Newtonian, power-law, Oldroyd-B, and FENE-P fluids are seamlessly integrated together in the new IB method via the lattice Boltzmann approach and they can be implemented in a single computer code.

4 Verification and validation

The numerical methods involved and their implementations used in the work have been verified and validated in different settings. The lattice Boltzmann method (D3Q19) and its implementation have been verified and validated in Zhu et al. [Zhu, Tretheway, Petzold et al. (2005)]. The lattice-Boltzmann immersed-boundary method (LB-IB) with its implementation for Newtonian fluid flows have been verified and validated in Zhu et al. [Zhu, He, Wang et al. (2011b)]. The LB-IB for power-law fluid is verified and validated in Zhu et al. [Zhu, Yu, Liu et al. (2017)]. The preliminary verification and validation of the LB-IB method for Oldroyd-B/FENE-P have been reported in a short letter [Zhu (2018)].

In this paper, the newly developped LB-IB method for polymeric flows are further tested on two new FFSI toy problems: a flexible sheet being flapped periodically at the middle and being rotated constantly at one edge in stationary Oldroy-B and FENE-P fluids in three dimensions. Many simulations with various dimensionless parameters indicate that the method is conditionally stable. Mesh refinement studies indicate the method is first-order accurate, which is consistent with the IB framework in general.

5 Test problems

In this section we consider three FFSI model problems. I) a power-law fluid flows around a flexible rectangular sheet fixed at the midline in a three-dimensional rectangular domain; II) a flexible rectangular sheet is flapped sideways (left and right) at the midline sinusoidally in a 3D rectangular box full of an Oldroyd-B; III) a flexible rectangular sheet is rotated constantly at one edge with a constant speed in a 3D rectangular box full of a FENE-P fluid.

In case I, the structure is initially stationary. The flow passes around it and causes it to bend and get aligned with the flow. No-slip boundary condition is applied on the top, bottom, front, and rear rigid walls. Constant velocity is specified at the inlet and outlet boundaries (in x-axis). In cases II and III, the fluid is initially stationary and the structure is forced to move. The active motions of the structures drive the fluid flow. Periodic boundary condition is applied along all directions of the computational domain. In all cases, the $x-$ axis points from left to right; the $y-$ axis points from front to rear; the $z-$ axis points from bottom to top. The sheets are composed of two groups of elastic fibers which can be compressed, stretched, and bent. The two groups of fibers are cross-linked and are orthogonal to each other initially. This type of FFSI problem possesses three significant dimensionless parameters: flow Reynolds number Re, structure bending modulus $\hat{K_b}$, and fluid Weissenberg number W_i (or exponent n for power-law fluid). Numerous simulations on the three model problems using various combinations of these parameters are performed to test the capability of the new method. Some representative simulation results are reported below for each case.

Case I) An elastic sheet with aspect ratio 1:2 (width versus length) is placed initially on the $y-z$ plane (i.e., vertical) in the middle of the box (in x, y, and z directions). Its midline is fixed in a power-law fluid flow and the sheet is free to move otherwise. This problem was intensively studied by Zhu et al. [Zhu, Yu, Liu et al. (2017)]. More simulations are performed and some typical results from different combination of values of $Re, \hat{K_b}, n$ are shown here. The left panel in Fig. 1 shows the position and shape of the sheet at several equally distributed time instants from a simulation with $Re = 80, \hat{K}b = 0.0001, n = 0.5$. The left most is the initial position (vertical and flat). The right most is the final position (curved). Starting from the initial configuration, the sheet moves and deforms with the flow, and finally sets down to a quasi-steady state. Note that the position/shape of the sheet partially overlap for some instants. The right panel in Fig. 1 shows streamlines of the flow field from a simulation with $Re = 120, \hat{K}b = 0.05, n = 0.6$. The gray surface is the

position and shape of the sheet. The streamlines start from the lower half plane of the inlet (using tens of uniformly spaced seeds). Notice the twisted curves behind the sheet. These streamlines come from the lower half plane at inlet and move to the upper half plane after past the sheet. This reveals the complicated flow patterns right behind the sheet.

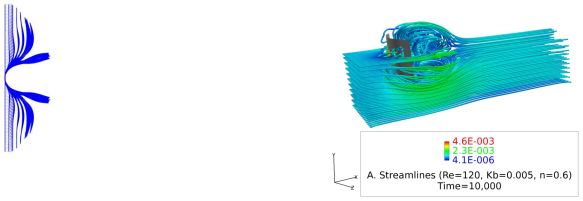

Figure 1: Position and shape of the sheet at several instants (left) and streamlines (right)

Case II) A deformable sheet of the same aspect ratio is initially placed the same way as in case I. Its midline is now forced to flap sinusoidally (on the $x-y$ plane along x-direction) in an Oldroyd-B fluid. The x-coordinate of the leading edge is given by $x(t) = Asin(\frac{2\pi t}{P})$. Here $x(t)$ is the x-coordinate of the sheet middle-line, A denotes prescribed amplitude of flapping, P denotes flapping period, and t denotes time. Some typical results from different combination of values of $Re, \hat{K}_b, Wi$ are given below. In Fig. 2 the left panel plots the shape of the sheet at several equally separated instants from a simulation with $Re = 40, \hat{K}b = 0.005, Wi = 0.1$. The left most is the initial position (vertical and flat). The rest is the shape (not physical position) of the sheet at several time instants within a period. Note that the sheet physical position (x-coordinate) is shifted horizontally by a constant for the purpose of displaying the shapes at multiple instants on the same panel. Starting from the initial position, the sheet moves and deforms with the flapping midline. Spontaneous motion of the sheet along y and z directions are not seen. The right panel in Fig. 2 shows streamlines of the flow field from a simulation with $Re = 60, \hat{K}b = 0.004, Wi = 0.1$. The gray surface (partially buried in the curves) at the center is the position and shape of the sheet. All streamlines start from a vertical plane (parallel to the initial position of the sheet) near the left boundary of the computational domain (using 25 uniformly spaced seeds). Notice the colors of the curves denote the velocity magnitude. The twisted curves around the sheet indicates the complexity of flow patterns in the vicinity of the structure.

Case III) An elastic sheet with aspect ratio of 1:4 (width versus length) is initially put on a horizontal plane of the x and y axes in the middle of the box in all three directions (x, y, and z). Its right edge is rotated constantly and periodically with a period P (on the $y-z$ plane anticlockwise) in a still FENE-P fluid. Again, the structure is not restricted elsewhere and is allowed to move freely in other directions. Some typical results from different combination of values of $Re, \hat{K}_b, Wi$ are displayed here. In Fig. 3 the left panel

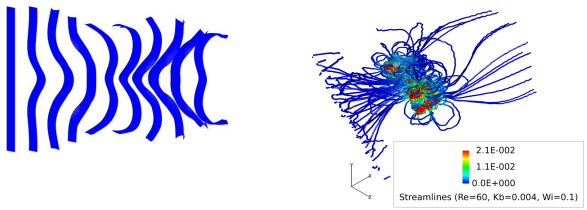

Figure 2: Shape of the sheet at several instants (left) and streamlines (right)

shows the shape/position of the sheet at a few equally distributed instants from a simulation with $Re = 10, \hat{Kb} = 0.005, Wi = 1.0$. The top most is the initial position (horizontal and flat). The remaining is the shape (not physical position) of the sheet at several time instants within a period. Note that the sheet vertical position is shifted down by a constant for the same purpose as in case II. We see that as the right edge is being rotated, the rest of the sheet follows the rotation motion. Due to flexibility (instead of being rigid), the leading edge (initially straight) deforms into a curve and the entire sheet deforms into a helical structure. As time goes by, more helical structures appear and they appear to move downstream (from righ to left) in an animation. Interestingly the entire sheet moves forward towards right boundary slowly. The right panel in Fig. 3 shows streamlines of the flow field from a simulation with $Re = 10, \hat{Kb} = 0.005, Wi = 1.0$. The gray surface (partially blocked by the curves) is the position and shape of the twisted sheet. All streamlines start from a horizontal plane parallel and close to the initial position of the sheet (20 uniformly spaced seeds). The colors of the curves denote the velocity magnitude. The tightly wound curves around the sheet indicate a rotating flow near the sheet.

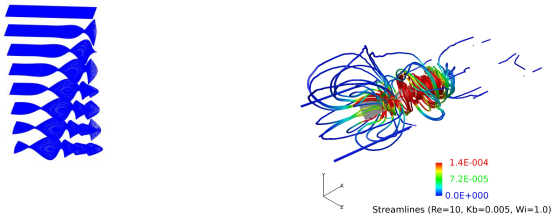

Figure 3: Shape of the sheet at several instants (left) and streamlines (right)

6 Summary

The existing immersed boundary (IB) framework has been extended in three dimensions to FFSI problems involving non-Newtonian fluids. The fluids may be power-law, Oldroyd-

B, or FENE-P. The viscous incompressible Navier-Stokes equations for the flow and the constitutive equations for the fluid (Oldroyd-B and FENE-P) are simultaneously solved with the lattice Boltzmann approaches by the D3Q19 and the D3Q7 models, respectively. The power-law is incorporated algebraically into the lattice Boltzmann flow model. The new method is tested on three FFSI toy problems: deformable sheets interacting with power-law, Oldroyd-B, and FENE-P fluids in three dimensions. Our results show that the new IB method is first-order accurate and conditionally stable.

Acknowledgment: The work is supported by the US National Science Foundation (NSF) through the research grant DMS-1522554. We thank the unknown Reviewers for their helpful suggestions and comments which have helped us.

References

Atzberger, P. J.; Kramer, P. R. (2008): Error analysis of a stochastic immersed boundary method incorporating thermal fluctuations. *Mathematics and Computers in Simulation*, vol. 79, no. 3, pp. 379-408.

Atzberger, P. J.; Kramer, P. R.; Peskin, C. S. (2007): A stochastic immersed boundary method for fluid-structure dynamics at microscopic length scales. *Journal of Computational Physics*, vol. 224, no. 2, pp. 1255-1292.

Barker, A. T.; Cai, X. C. (2010): Scalable parallel methods for monolithic coupling in fluid-structure interaction with application to blood flow modeling. *Journal of Computational Physics*, vol. 229, no. 3, pp. 642-659.

Boffi, D.; Gastaldi, L. (2003): A finite element approach for the immersed boundary method. *Computers & Structures*, vol. 81, no. 8-11, pp. 491-501.

Boffi, D.; Gastaldi, L.; Heltai, L.; Peskin, C. S. (2008): On the hyper-elastic formulation of the immersed boundary method. *Computer Methods in Applied Mechanics and Engineering*, vol. 197, no. 25-28, pp. 2210-2231.

Cheng, Y.; Zhang, H. (2010): Immersed boundary method and lattice boltzmann method coupled fsi simulation of mitral leaflet flow. *Computers & Fluids*, vol. 39, no. 5, pp. 871-881.

Cheng, Y.; Zhu, L.; Zhang, C. (2014): Numerical study of stability and accuracy of the immersed boundary method coupled to the lattice boltzmann bgk model. *Communications in Computational Physics*, vol. 16, no. 1, pp. 136-168.

Chrispell, J.; Cortez, R.; Khismatullin, D.; Fauci, L. (2011): Shape oscillations of a droplet in an oldroyd-b fluid. *Physica D: Nonlinear Phenomena*, vol. 240, no. 20, pp. 1593-1601.

Chrispell, J. C.; Fauci, L. J.; Shelley, M. (2013): An actuated elastic sheet interacting with passive and active structures in a viscoelastic fluid. *Physics of Fluids*, vol. 25, no. 1.

Cortez, R. (2000): A vortex/impulse method for immersed boundary motion in high reynolds number flows. *Journal of Computational Physics*, vol. 160, no. 1, pp. 385-400.

Cottet, G. H.; Maitre, E. (2006): A level set method for fluid-structure interactions with immersed surfaces. *Mathematical Models and Methods in Applied Sciences*, vol. 16, no. 3, pp. 415-438.

Donea, J.; Giuliani, S.; Halleux, J. (1982): An arbitrary lagrangian-eulerian finite element method for transient dynamic fluid-structure interactions. *Computer Methods in Applied Mechanics and Engineering*, vol. 33, no. 1, pp. 689-723.

Fai, T. G.; Griffith, B. E.; Mori, Y.; Peskin, C. S. (2013): Immersed boundary method for variable viscosity and variable density problems using fast constant-coefficient linear solvers i: numerical method and results. *SIAM Journal on Scientific Computing*, vol. 35, no. 5, pp. B1132-B1161.

Fai, T. G.; Griffith, B. E.; Mori, Y.; Peskin, C. S. (2014): Immersed boundary method for variable viscosity and variable density problems using fast constant-coefficient linear solvers ii: theory. *SIAM Journal on Scientific Computing*, vol. 36, no. 3, pp. 589-621.

Fauci, L. J.; Fogelson, A. L. (1993): Truncated newton methods and the modeling of complex immersed elastic structures. *Communications on Pure and Applied Mathematics*, vol. 46, no. 6, pp. 787-818.

Feng, Z. G.; Michaelides, E. E. (2004): The immersed boundary-lattice boltzmann method for solving fluid-particles interaction problems. *Journal of Computational Physics*, vol. 195, no. 2, pp. 602-628.

Feng, Z. G.; Michaelides, E. E. (2005): Proteus: a direct forcing method in the simulations of particulate flows. *Journal of Computational Physics*, vol. 202, no. 1, pp. 20-51.

Glimm, J.; Grove, J. W.; Li, X. L.; Shyue, K. M.; Zeng, Y. et al. (1998): Three-dimensional front tracking. *SIAM Journal on Scientific Computing*, vol. 19, no. 3, pp. 703-727.

Glowinski, R.; Pan, T. F.; Periaux, J. (1994): A fictitious domain method for dirichlet problem and applications. *Computer Methods in Applied Mechanics and Engineering*, vol. 111, no. 3, pp. 283-303.

Glowinski, R.; Pan, T. W.; Periaux, J. (1994): A fictitious domain method for external incompressible viscous flow modeled by navier-stokes equations. *Computer Methods in Applied Mechanics and Engineering*, vol. 112, no. 1, pp. 133-148.

Griffith, B. E.; Hornung, R. D.; McQueen, D. M.; Peskin, C. S. (2007): An adaptive, formally second order accurate version of the immersed boundary method. *Journal of Computational Physics*, vol. 223, no. 1, pp. 10-49.

Griffith, B. E.; Luo, X. (2012): Hybrid finite difference/finite element version of the immersed boundary method. *Submitted in Revised Form*.

Griffith, B. E.; Peskin, C. S. (2005): On the order of accuracy of the immersed boundary method: higher order convergence rates for sufficiently smooth problems. *Journal of Computational Physics*, vol. 208, no. 1, pp. 75-105.

Guo, Z.; Shu, C. (2013): *Lattice Boltzmann Method and Its Applications in Engineering*, volume 3. World Scientific.

Guo, Z.; Zheng, C.; Shi, B. (2002): Discrete lattice effects on the forcing term in the lattice boltzmann method. *Physical Review E*, vol. 65, no. 4.

Hao, J.; Zhu, L. (2010): A lattice boltzmann based implicit immersed boundary method for fluid-structure interaction. *Computers & Mathematics with Applications*, vol. 59, no. 1, pp. 185-193.

Hao, J.; Zhu, L. (2011): A three dimensional implicit immersed boundary method with application. *Theoretical and Applied Mechanics Letters*, vol. 1, no. 6.

Hou, T. Y.; Li, Z.; Osher, S.; Zhao, H. (1997): A hybrid method for moving interface problems with application to the hele-shaw flow. *Journal of Computational Physics*, vol. 134, no. 2, pp. 236-252.

Hou, T. Y.; Shi, Z. (2008): An efficient semi-implicit immersed boundary method for the navier-stokes equations. *Journal of Computational Physics*, vol. 227, no. 20, pp. 8968-8991.

Hron, J.; Turek, S. (2006): A monolithic fem/multigrid solver for an ale formulation of fluid-structure interaction with applications in biomechanics. *Fluid-Structure Interaction*, pp. 146-170.

Hua, R. N.; Zhu, L.; Lu, X. Y. (2014): Numerical investigation of the dynamics of a flexible filament in the wake of cylinder. *Advances in Applted Mathematics and Mechanics*, vol. 6, no. 4, pp. 478-493.

Huang, H.; Sukop, M.; Lu, X. (2015): *Multiphase Lattice Boltzmann Methods: Theory and Application*. John Wiley & Sons.

Hübner, B.; Walhorn, E.; Dinkler, D. (2004): A monolithic approach to fluid-structure interaction using space-time finite elements. *Computer Methods in Applied Mechanics and Engineering*, vol. 193, no. 23-26, pp. 2087-2104.

Hughes, T. J.; Liu, W. K.; Zimmermann, T. K. (1981): Lagrangian-eulerian finite element formulation for incompressible viscous flows. *Computer Methods in Applied Mechanics and Engineering*, vol. 29, no. 3, pp. 329-349.

Iaccarino, G.; Verzicco, R. (2003): Immersed boundary technique for turbulent flow simulations. *Applied Mechanics Reviews*, vol. 56, no. 3, pp. 331-347.

Jin, C.; Xu, K. (2008): Numerical study of the unsteady aerodynamics of freely falling plates. *Communications in Computational Physics*, vol. 3, no. 4, pp. 834-851.

Junk, M. (2001): A finite difference interpretation of the lattice boltzmann method. *Numerical Methods for Partial Differential Equations: An International Journal*, vol. 17, no. 4, pp. 383-402.

Kim, Y.; Peskin, C. S. (2007): Penalty immersed boundary method for an elastic boundary with mass. *Physics of Fluids (1994-Present)*, vol. 19, no. 5, 053103.

Kim, Y.; Peskin, C. S. (2016): A penalty immersed boundary method for a rigid body in fluid. *Physics of Fluids*, vol. 28, no. 3.

Lai, M. C.; Peskin, C. S. (2000): An immersed boundary method with formal second-order accuracy and reduced numerical viscosity. *Journal of computational Physics*, vol. 160, no. 2, pp. 705-719.

Lallemand, P.; Luo, L. S. (2003): Lattice boltzmann method for moving boundaries. *Journal of Computational Physics*, vol. 184, no. 2, pp. 406-421.

Lee, P.; Griffith, B. E.; Peskin, C. S. (2010): The immersed boundary method for advection-electrodiffusion with implicit timestepping and local mesh refinement. *Journal of Computational Physics*, vol. 229, no. 13, pp. 5208-5227.

Leveque, R. J.; Li, Z. (1994): The immersed interface method for elliptic equations with discontinuous coefficients and singular sources. *SIAM Journal on Numerical Analysis*, vol. 31, no. 4, pp. 1019-1044.

LeVeque, R. J.; Li, Z. (1997): Immersed interface methods for stokes flow with elastic boundaries or surface tension. *SIAM Journal on Scientific Computing*, vol. 18, no. 3, pp. 709-735.

Li, Z.; Lai, M. C. (2001): The immersed interface method for the navier-stokes equations with singular forces. *Journal of Computational Physics*, vol. 171, no. 2, pp. 822-842.

Lim, S.; Ferent, A.; Wang, X. S.; Peskin, C. S. (2008): Dynamics of a closed rod with twist and bend in fluid. *SIAM Journal on Scientific Computing*, vol. 31, no. 1, pp. 273-302.

Liu, N.; Peng, Y.; Liang, Y.; Lu, X. (2012): Flow over a traveling wavy foil with a passively flapping flat plate. *Physical Review E*, vol. 85, no. 5.

Liu, W. K.; Kim, D. W.; Tang, S. (2007): Mathematical foundations of the immersed finite element method. *Computational Mechanics*, vol. 39, no. 3, pp. 211-222.

Ma, J.; Wang, Z.; John, Y.; Lai, J.; Sui, Y.; Tian, F. (2018): An immersed boundary lattice Boltzmann method for fluid-structure-interaction involving viscoelastic fluids. *Private Communication*.

Malaspinas, O.; Fiétier, N.; Deville, M. (2010): Lattice boltzmann method for the simulation of viscoelastic fluid flows. *Journal of Non-Newtonian Fluid Mechanics*, vol. 165, no. 23, pp. 1637-1653.

McCracken, M.; Peskin, C. (1980): A vortex method for blood flow through heart valves. *Journal of Computational Physics*, vol. 35, no. 2, pp. 183-205.

Mittal, R.; Iaccarino, G. (2005): Immersed boundary methods. *Annual Review of Fluid Mechanics*, vol. 37, pp. 239-261.

Mokbel, D.; Abels, H.; Aland, S. (2018): A phase-field model for fluid-structure-interaction. arxiv:1803.02354.

Mori, Y.; Peskin, C. S. (2008): Implicit second-order immersed boundary methods with boundary mass. *Computer Methods in Applied Mechanics and Engineering*, vol. 197, no. 25, pp. 2049-2067.

Newren, E. P.; Fogelson, A. L.; Guy, R. D.; Kirby, R. M. (2008): A comparison of implicit solvers for the immersed boundary equations. *Computer Methods in Applied Mechanics and Engineering*, vol. 197, no. 25-28, pp. 2290-2304.

Niu, X.; Shu, C.; Chew, Y.; Peng, Y. (2006): A momentum exchange-based immersed boundary-lattice boltzmann method for simulating incompressible viscous flows. *Physics Letters A*, vol. 354, no. 3, pp. 173-182.

Oldroyd, J. (1950): On the formulation of rheological equations of state. *Proceedings of the Royal Society of London. Series A. Mathematical and Physical Sciences*, vol. 200, no. 1063, pp. 523-541.

Peskin, C.; McQueen, D. (1996): *Fluid Dynamics of the Heart and Its Valves, in Case Studies in Mathematical Modeling: Ecology, Physiology, and Cell Biology*. Prentice-Hall, Englewood Cliffs, NJ.

Peskin, C. S. (1972): Flow patterns around heart valves: a numerical method. *Journal of Computational Physics*, vol. 10, no. 2, pp. 252-271.

Peskin, C. S. (1973): Flow patterns around heart valves: a digital computer method for solving the equations of motion. *IEEE Transactions on Biomedical Engineering*, , no. 4, pp. 316-317.

Peskin, C. S. (1977): Numerical analysis of blood flow in the heart. *Journal of Computational Physics*, vol. 25, no. 3, pp. 220-252.

Peskin, C. S.; Printz, B. F. (1993): Improved volume conservation in the computation of flows with immersed elastic boundaries. *Journal of Computational Physics*, vol. 105, no. 1, pp. 33-46.

Peterlin, A. (1961): Streaming birefringence of soft linear macromolecules with finite chain length. *Polymer*, vol. 2, pp. 257-264.

Qian, Y. H. (1990): Lattice gas and lattice kinetic theory applied to the navier-stokes equations. *Doktorarbeit, Universite Pierre et Marie Curie, Paris*.

Roma, A. M.; Peskin, C. S.; Berger, M. J. (1999): An adaptive version of the immersed boundary method. *Journal of Computational Physics*, vol. 153, no. 2, pp. 509-534.

Rosar, M.; Peskin, C. S. (2001): Fluid flow in collapsible elastic tubes: a three-dimensional numerical model. *New York Journal of Mathematics*, vol. 7, pp. 281-302.

Shu, C.; Liu, N.; Chew, Y. T. (2007): A novel immersed boundary velocity correction-lattice boltzmann method and its application to simulate flow past a circular cylinder. *Journal of Computational Physics*, vol. 226, no. 2, pp. 1607-1622.

Stockie, J. M. (2009): Modelling and simulation of porous immersed boundaries. *Computers & Structures*, vol. 87, no. 11-12, pp. 701-709.

Strychalski, W.; Copos, C. A.; Lewis, O. L.; Guy, R. D. (2015): A poroelastic immersed boundary method with applications to cell biology. *Journal of Computational Physics*, vol. 282, pp. 77-97.

Succi, S. (2018): *The Lattice Boltzmann Equation: For Complex States of Flowing Matter*. Oxford University Press.

Sulsky, D.; Chen, Z.; Schreyer, H. L. (1994): A particle method for history-dependent materials. *Computer Methods in Applied Mechanics and Engineering*, vol. 118, no. 1, pp. 179-196.

Sulsky, D.; Zhou, S. J.; Schreyer, H. L. (1995): Application of a particle-in-cell method to solid mechanics. *Computer Physics Communications*, vol. 87, no. 1, pp. 236-252.

Sun, P.; Xu, J.; Zhang, L. (2014): Full eulerian finite element method of a phase field model for fluid-structure interaction problem. *Computers & Fluids*, vol. 90, pp. 1-8.

Shen, S.; Doolen, G. D. (1998): Lattice boltzmann method for fluid flows. *Annual Review of Fluid Mechanics*, vol. 30, pp. 329.

Taira, K.; Colonius, T. (2007): The immersed boundary method: a projection approach. *Journal of Computational Physics*, vol. 225, no. 2, pp. 2118-2137.

Tian, F. B. (2016): Deformation of a capsule in a power-law shear flow. *Computational and Mathematical Methods in Medicine*, vol. 2016.

Tian, F. B.; Luo, H.; Zhu, L.; Liao, J. C.; Lu, X. Y. (2011): An efficient immersed boundary-lattice boltzmann method for the hydrodynamic interaction of elastic filaments. *Journal of Computational Physics*, vol. 230, no. 19, pp. 7266-7283.

Wang, L.; Currao, G. M.; Han, F.; Neely, A. J.; Young, J. et al. (2017): An immersed boundary method for fluid-structure interaction with compressible multiphase flows. *Journal of Computational Physics*, vol. 346, pp. 131-151.

Wang, X.; Liu, W. K. (2004): Extended immersed boundary method using fem and rkpm. *Computer Methods in Applied Mechanics and Engineering*, vol. 193, no. 12, pp. 1305-1321.

Wang, X. S. (2006): From immersed boundary method to immersed continuum methods. *International Journal for Multiscale Computational Engineering*, vol. 4, no. 1.

Wick, T. (2016): Coupling fluid-structure interaction with phase-field fracture. *Journal of Computational Physics*, vol. 327, pp. 67-96.

Wolf-Gladrow, D. A. (2000): *Lattice-Gas Cellular Automata and Lattice Boltzmann Models: An Introduction*. No. 1725. Springer.

Wu, J.; Shu, C. (2009): Implicit velocity correction-based immersed boundary-lattice boltzmann method and its applications. *Journal of Computational Physics*, vol. 228, no. 6, pp. 1963-1979.

Wu, J.; Shu, C.; Zhang, Y. (2010): Simulation of incompressible viscous flows around moving objects by a variant of immersed boundary-lattice boltzmann method. *International Journal of Numerical Methods for Heat and Fluid Flow*, vol. 62, no. 3, pp. 327-354.

Xu, J. J.; Li, Z.; Lowengrub, J.; Zhao, H. (2006): A level-set method for interfacial flows with surfactant. *Journal of Computational Physics*, vol. 212, no. 2, pp. 590-616.

Yang, K.; Sun, P.; Wang, L.; Xu, J.; Zhang, L. (2016): Modeling and simulations for fluid and rotating structure interactions. *Computer Methods in Applied Mechanics and Engineering*, vol. 311, pp. 788-814.

Zhang, C.; Cheng, Y.; Zhu, L.; Wu, J. (2016): Accuracy improvement of the immersed boundary-lattice boltzmann coupling scheme by iterative force correction. *Computers & Fluids*, vol. 124, pp. 246-260.

Zhang, L.; Gerstenberger, A.; Wang, X.; Liu, W. K. (2004): Immersed finite element method. *Computer Methods in Applied Mechanics and Engineering*, vol. 193, no. 21, pp. 2051-2067.

Zheng, X.; Karniadakis, G. (2016): A phase-field/ale method for simulating fluid-structure interactions in two-phase flow. *Computer Methods in Applied Mechanics and Engineering*, vol. 309, pp. 19-40.

Zhu, L. (2018): A three-dimensional immersed boundary method for non-newtonian fluids. *Theoretical and Applied Mechanics Letters*, vol. 8, no. 3, pp. 193-196.

Zhu, L.; Chin, R. C. (2008): Simulation of elastic filaments interacting with a viscous pulsatile flow. *Computer Methods in Applied Mechanics and Engineering*, vol. 197, no. 25-28, pp. 2265-2274.

Zhu, L.; He, G.; Wang, S.; Miller, L.; Zhang, X. et al. (2011): An immersed boundary method based on the lattice boltzmann approach in three dimensions, with application. *Computers & Mathematics with Applications*, vol. 61, no. 12, pp. 3506-3518.

Zhu, L.; Peskin, C. S. (2002): Simulation of a flapping flexible filament in a flowing soap film by the immersed boundary method. *Journal of Computational Physics*, vol. 179, no. 2, pp. 452-468.

Zhu, L.; Tretheway, D.; Petzold, L.; Meinhart, C. (2005): Simulation of fluid slip at 3d hydrophobic microchannel walls by the lattice boltzmann method. *Journal of Computational Physics*, vol. 202, no. 1, pp. 181-195.

Zhu, L.; Yu, X.; Liu, N.; Cheng, Y.; Lu, X. (2017): A deformable plate interacting with a non-newtonian fluid in three dimensions. *Physics of Fluids*, vol. 29, no. 8.